Polymer 50 (2009) 2273–2280

Contents lists available at ScienceDirect

Polymer

journal homepage: www.elsevier.com/locate/polymer

Effects of substrate roughness on the orientation of cylindrical domains in thin films of a polystyrene–poly(methylmethacrylate) diblock copolymer studied using atomic force microscopy and cyclic voltammetry

Helene C. Maire, Shaida Ibrahim, Yongxin Li, Takashi Ito*

Department of Chemistry, Kansas State University, 213 CBC Building, Manhattan, KS 66506-0401, USA

ARTICLE INFO

Article history:
Received 30 December 2008
Received in revised form
24 February 2009
Accepted 1 March 2009
Available online 11 March 2009

Keywords:
Block copolymer
Atomic force microscopy
Cyclic voltammetry

ABSTRACT

This paper describes the orientation of cylindrical domains in thin films of a polystyrene–poly(methylmethacrylate) diblock copolymer (PS-*b*-PMMA; 0.3 as the PMMA volume fraction) on gold and oxide-coated Si substrates having different surface roughness. Atomic force microscopy images of PS-*b*-PMMA films having thickness similar to the domain periodicity permitted us to study the effects of substrate roughness and block affinity on domain orientation. PS-*b*-PMMA films on gold substrates showed metastable vertical domain orientation that was attained more slowly on rougher substrates. In contrast, the domains were horizontally oriented on oxide-coated Si regardless of surface roughness and the annealing conditions examined. In addition, cyclic voltammetry data for PS-*b*-PMMA films on gold substrates whose PMMA domains were etched suggested that the metastable vertically oriented domains reached the underlying substrates. These results indicate that PS-*b*-PMMA films containing vertically oriented cylindrical domains can be obtained by using rough gold substrates upon annealing under controlled conditions.

1. Introduction

This paper reports the effects of substrate surface roughness and block affinity on the orientation of cylindrical domains in thin films of a polystyrene–poly(methylmethacrylate) diblock copolymer (PS-*b*-PMMA; 0.3 as the volume fraction of PMMA). Thin films of asymmetric PS-*b*-PMMA with controlled thicknesses (20 ~ 200 nm) were prepared on gold and oxide-coated Si substrates having different surface roughness. The orientation of cylindrical domains at the free surface of PS-*b*-PMMA films was measured using atomic force microscopy (AFM). In addition, the extent of vertical domain orientation inside a PS-*b*-PMMA film was inferred using cyclic voltammetry (CV) on gold substrates coated with PS-*b*-PMMA films whose PMMA domains were chemically removed.

Block copolymers (BCPs) [1–4] containing self-organized nanoscale domains have recently been employed to fabricate masks for lithography [5], templates for metal or silica nanowire synthesis [6,7], templates for nanoparticle deposition [8,9], and filtration membranes for viruses [10,11]. In particular, BCPs that form cylindrical domains of the minor component [1–4] have been used to fabricate monoliths containing an array of uniform nanopores by chemically etching the minor component [3,4,12]. For the aforementioned applications, it is important to control the diameter and alignment of the cylindrical domains in BCP monoliths. Whereas the domain diameter can be controlled by changing the molecular weight of the BCP [1–4], it is often challenging to control the alignment of the domains. In a BCP film supported by a substrate, the orientation of cylindrical domains is strongly affected by interactions at the BCP–substrate interface and at the free surface of the BCP film. Preferential wetting of one fragment at an interface leads to horizontal domain orientation. To align cylindrical domains vertically to an underlying substrate, the substrate surface has often been chemically tailored to balance the affinities of the BCP fragments [13,14]. For example, such neutralized surfaces for PS-*b*-PMMA were obtained on hydrogen-terminated Si [15], on substrates modified with organosilane self-assembled monolayers [16], and on substrates covalently modified with a brush layer of a PS–PMMA random copolymer having an appropriate volume fraction [13,17]. In addition to controlling the surface affinity of the underlying substrates, several approaches have been simultaneously employed to improve the vertical alignment of cylindrical PMMA domains in a PS-*b*-PMMA film, including optimization of film thickness [18,19], addition of PMMA homopolymers [20], control of solvent-evaporation conditions [21], and electric field application during annealing [6,12,22].

* Corresponding author. Tel.: +1 785 532 1451; fax: +1 785 532 6666.
E-mail address: ito@ksu.edu (T. Ito).

0032-3861/$ – see front matter © 2009 Elsevier Ltd. All rights reserved.
doi:10.1016/j.polymer.2009.03.002

Recently, Sivaniah and coworkers experimentally demonstrated that the roughness of a substrate surface induced the vertical alignment of lamellar PMMA domains in thin films of symmetric PS-*b*-PMMA [23–25]. The domain orientation was influenced by the lateral periodicity and vertical amplitude of the surface corrugations of an underlying substrate as well as the periodicity of the BCP domains (L_0). The roughness-induced vertical alignment of BCP domains was theoretically explained using a model based on the distortion of aligned domain structures by the rough surface [26–28]. The roughness-induced domain alignment provides a simple means for preparing thin PS-*b*-PMMA films containing vertically-aligned PMMA domains, because it does not require the chemical neutralization of the substrate surface [23,24].

In this study, we investigated the effects of substrate surface roughness and block affinity on the orientation of PMMA domains in thin films of cylinder-forming, asymmetric PS-*b*-PMMA instead of lamella-forming, symmetric PS-*b*-PMMA. The orientation of cylindrical PMMA domains in PS-*b*-PMMA films having different thicknesses and annealed under different conditions was assessed using AFM and CV. The vertical orientation of cylindrical PMMA domains could be obtained on gold substrates covered with nanoscale grains under controlled annealing conditions. In contrast, the cylindrical domains were oriented horizontally on oxide-coated Si substrates regardless of substrate roughness and the annealing conditions examined.

2. Experimental

2.1. Chemicals and materials

PS-*b*-PMMA (average molecular weights of PS and PMMA: 39,800 and 17,000, respectively; polydispersity: 1.06) was purchased from Polymer Source and used as received. Toluene (Fischer Chemical), HF (Acros Organics), potassium nitrate (Fischer Chemical) and 1,1′-ferrocenedimethanol ($Fc(CH_2OH)_2$; Aldrich) were used without further purification. Planar Si (100) wafers (p-type) were purchased from University Wafer (South Boston, MA). Gold-coated Si wafers (Au/Si), which were prepared via sputtering 10-nm Ti followed by 200-nm Au onto Si (100) wafers, were purchased from LGA Thin Films (Foster City, CA). Gold-coated glass slides (Au/glass), which were prepared by electron-beam deposition of 100-nm Au onto aluminosilicate glass microscope slides with a thin Ti adhesion layer, were purchased from Platypus Technologies (Madison, WI). Solutions used for electrochemical measurements were prepared with water having an 18 MΩ cm or higher resistivity (Barnstead Nanopure System).

2.2. Substrate preparation

All Si and Au substrates (ca. $1 \times 1\ cm^2$ for AFM studies and $1.5 \times 2\ cm^2$ for electrochemical measurements) were sonicated in ethanol and then cleaned using a Novascan PSD-UVT UV-Ozone system in air for 30 min. Roughened oxide-coated Si substrates were prepared by immersing the cleaned Si substrates in a 2% w/w ammonium fluoride solution [29] for 20 min, with sonication for the first 10 min. The roughened Si substrates were re-oxidized in a UV–Ozone system for 30 min in air.

2.3. Preparation of PS-b-PMMA thin films

A thin film of PS-*b*-PMMA was prepared on a substrate via spin-coating (2000 rpm, 30 s) from its toluene solution. The thickness of a polymer film was controlled by varying the concentration of the toluene solution in the range from 0.5 to 3% (w/w). The polymer-coated substrates were annealed in an Isotemp vacuum oven Model 280a at 170 or 190 °C in vacuum (0.3 Torr) for 60 ~ 210 h to allow the formation of cylindrical PMMA domains in the film. For CV measurements, the PMMA domains in PS-*b*-PMMA films on Au substrates were degraded by UV irradiation for 80 min using the Novascan PSD-UVT UV-Ozone system under Ar atmosphere, and then removed by sonication in glacial acetic acid (AcOH) for 30 min. The UV-irradiated PS-*b*-PMMA films were not damaged by the sonication process probably due to the cross-linking of the PS matrix during the UV irradiation [30].

2.4. Characterization of substrates and PS-b-PMMA films

Water contact angles (θ^{water}) were measured to assess the cleanness of a substrate prior to the polymer film deposition. A water droplet (2 μL) was deposited onto a substrate surface, and the angles at the two opposite water–substrate interfaces were measured within 30 s after depositing the drop [31]. The thickness of an annealed PS-*b*-PMMA thin film (t) was measured using a J.A. Woollam alpha-SE spectroscopic ellipsometer. The thickness of a PS-*b*-PMMA film, measured using spectroscopic ellipsometry, was validated by comparing with those measured using profilometry (t_p): $t/t_p = 1.05 \pm 0.11$ for 21 films having thickness of ≤800 nm. AFM images of sample surfaces were measured by Tapping-mode imaging in air, using a Digital Instruments Multimode AFM with Nanoscope IIIa electronics. Tapping-mode AFM probes from Applied Nanostructures (cantilever length: 125 μm; force constant: 40 N/m; resonance frequency: 300 kHz) were used. CV measurements were performed in a three-electrode cell using a CH Instruments model 618B electrochemical analyzer, as reported previously [32]. The values and errors reported here are the averages and 90% confidence limits, respectively, obtained from multiple measurements on multiple samples.

3. Results and discussion

3.1. Surface roughness and cleanness of planar substrates

In this study, four types of planar substrates were employed as supports for PS-*b*-PMMA films (Fig. 1): Au substrates prepared on Si wafer via sputtering (Au/Si; Fig. 1(a)), Au substrates prepared on aluminosilicate glass via electron-beam deposition (Au/glass; Fig. 1(b)), smooth oxide-coated Si substrates (s-SiO_2/Si; Fig. 1(c)) and roughened oxide-coated Si substrates (r-SiO_2/Si; Fig. 1(d)). Table 1 summarizes the root-mean-square (RMS) vertical displacement (R), average grain diameter (d_g) and water contact angle (θ^{water}) of these substrates. s-SiO_2/Si was very smooth, whereas the other substrates showed nanoscale grains on their surfaces. In addition, the grain size and the roughness amplitude were largely different between Au/Si and Au/glass. The gold and Si substrates with different roughness allowed us to study the influences of substrate surface roughness on domain orientation in PS-*b*-PMMA films. The θ^{water} values of the gold surfaces were similar to those reported previously [33], and the very low θ^{water} values ($\approx 10°$) of the SiO_2/Si surfaces indicated the presence of thick oxide layers [34].

3.2. Effects of PS-b-PMMA film thickness on PMMA domain orientation

Since the PMMA volume fraction of the PS-*b*-PMMA employed here was 0.3, annealed PS-*b*-PMMA films contain self-assembled cylindrical domains of the minor PMMA fragments. Fig. 2 shows Tapping-mode AFM images of PS-*b*-PMMA thin films having different thicknesses on (a) Au/Si, (b) Au/glass, (c) s-SiO_2/Si and (d)

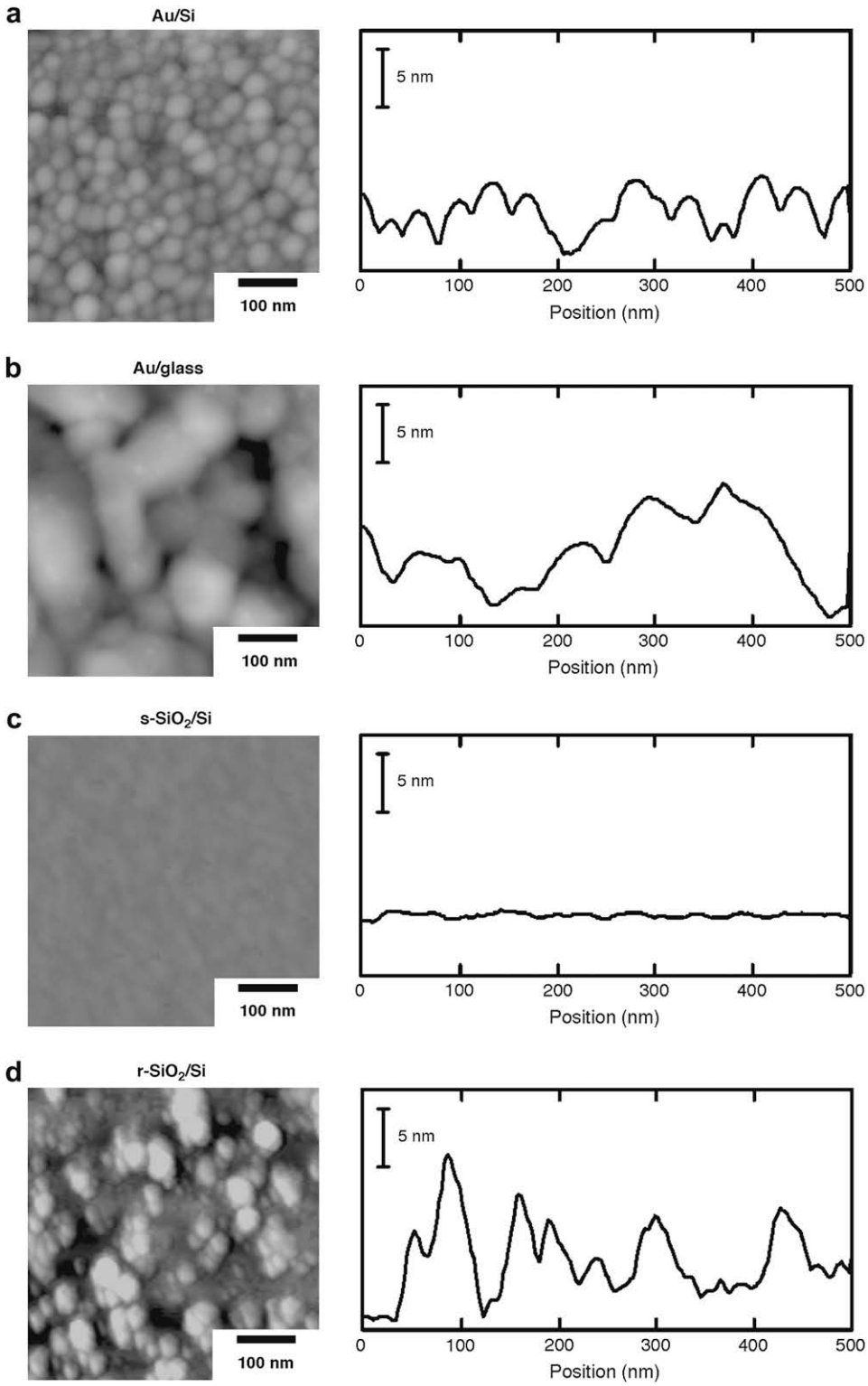

Fig. 1. AFM images (500×500 nm^2) of the cleaned surfaces of (a) Au/Si, (b) Au/glass, (c) s-SiO_2/Si and (d) r-SiO_2/Si. A typical cross-sectional profile of each sample surface is also given.

r-SiO_2/Si that were annealed at 170 °C for 60 h in vacuum. The domain periodicity (L_0) [1] of the PS-*b*-PMMA employed was ca. 35 nm. Samples were classified based on the ellipsometric thickness of the PS-*b*-PMMA films (t): (1) t is slightly smaller than the domain periodicity ($t = 17 \sim 24$ nm; left), (2) similar to L_0 ($t = 32 \sim 42$ nm; center), and (3) much larger than L_0 ($t = 120 \sim 177$ nm; right). These images clearly show that the surface features of PS-*b*-PMMA films were strongly affected by film thickness and underlying substrate.

When t was much larger than L_0 (Fig. 2, right raw), circular dots indicating cylindrical PMMA domains oriented vertically to the film surface were observed on the four types of substrates. The vertical domain orientation at the free surface probably

Table 1
Surface root-mean-square roughness (R), grain diameter on the surface (d_g) and water contact angle (θ^{water}) of the substrate surfaces used in this study.

Substrate	R (nm)[a]	d_g (nm)[b]	θ^{water} (°)[c]
s-SiO_2/Si	0.2 ± 0.0	–[d]	9 ± 2
r-SiO_2/Si	1.8 ± 0.5	40 ± 5	9 ± 1
Au/Si	1.4 ± 0.2	36 ± 5	43 ± 1
Au/glass	3.1 ± 0.4	132 ± 13	33 ± 2

[a] Average and 90% confidence limit of the root-mean-square (RMS) vertical displacement of at least three separate samples.
[b] The average and 90% confidence limit of the diameters of surface grains obtained from line profiles of AFM images.
[c] Average and 90% confidence limit, determined from at least three separate samples.
[d] The surfaces were too smooth to recognize the grains in the line profiles of AFM images.

reflected the nearly balanced affinity of the two polymer fragments at the polymer–vacuum interface, as suggested by the similar surface tension values of PS and PMMA at 150 °C (31.4 and 31.2 mN/m, respectively) [35]. The density of the vertical domains exposed to the surface was similar on the four substrates, but was slightly smaller than the maximum density of the hexagonal domains calculated from L_0 (ca. 900 domains/μm^2). The smaller domain density may reflect the slightly higher affinity of PS to vacuum [36]. These results indicate that the PS-*b*-PMMA films of $t \gg L_0$ are not suitable for demonstrating the influence of substrate properties on the orientation of cylindrical PMMA domains.

In contrast, AFM images of PS-*b*-PMMA films at $t < L_0$ and $t \approx L_0$ were different according to the substrates, suggesting that the domain orientation at the free surface of these thin films mainly reflected interactions at the polymer–substrate interface.

On Au/Si, vertical domains without any island structures were observed at $t < L_0$ and $t \approx L_0$ (Fig. 2(a), left and center), suggesting that the cylindrical PMMA domains on Au/Si were oriented vertically to the polymer–vacuum interface. Circular dots corresponding to vertical PMMA domains were observed at $t \approx L_0$ on Au/glass (Fig. 2(b), center). However, these circular dots distributed non-uniformly and at a density lower than half of that on Au/Si (Fig. 2(a), center). These observations suggest that the roughness of these gold substrates inhibits the horizontal orientation of the cylindrical domains and thus gives vertically oriented domains under the annealing conditions examined. Although it has been reported that gold surface is preferentially wetted by PS fragments [37,38], the difference in the affinity of PS and PMMA to the gold surface may not be so large [23]. An AFM image at $t < L_0$ on Au/glass (Fig. 2(b), left) did not show the domain morphology of PS-*b*-PMMA and instead showed the contour reflecting the surface structure of the substrate (Fig. 1(b)). The different domain morphologies on Au/Si and Au/glass probably reflected the kinetics of domain formation and orientation influenced by the substrate roughness (see 3.3) [24].

On the other hand, PMMA domains were horizontally oriented at $t \leq L_0$ on s-SiO_2/Si (Fig. 2(c)) and r-SiO_2/Si (Fig. 2(d)). The horizontal domains formed island structures in PS-*b*-PMMA films at $t < L_0$ (Fig. 2(c) and (d), left) and covered the whole surface at $t \approx L_0$ (Fig. 2(c) and (d), center) [1,8,39]. These observations are consistent with the commensurability effects [1,13]. These results indicate that the roughness did not significantly affect the domain orientation on SiO_2/Si substrates. The negligible effect of the surface roughness on oxide-coated Si surface is probably due to the much higher affinity of the PMMA fragments to the underlying oxidized Si surface [1]. This is probably because of the hydrogen bond interactions between surface Si–OH groups and the ester moieties of PMMA [39,40].

In summary, under the annealing conditions employed here, the domain orientation at the free surface of a PS-*b*-PMMA film at $t \leq L_0$ reflected interactions between the polymer fragments and substrate surface, whereas that at $t \gg L_0$ resulted from the balanced affinity of the polymer fragments at the polymer–vacuum interface. These results mean that the domain orientations, observed with AFM, were competitively determined by interfacial interactions at the polymer–vacuum and polymer–substrate interfaces, giving the thickness-dependent domain orientation. These conclusions could be obtained by systematically investigating domain orientation at the free film surface by varying film thickness on the same substrate and by using films of similar thickness on different substrates.

3.3. Effects of the annealing conditions on PMMA domain orientation in thin PS-*b*-PMMA films

As shown in Fig. 2(a) and (b), the substrate roughness induced the vertical orientation of cylindrical PMMA domains on gold. However, the roughness amplitudes of these substrates (Fig. 1(a) and (b)) were similar to those of substrates that showed metastable perpendicular orientation of lamellar microdomains in films of symmetric PS-*b*-PMMA [24]. On such moderately rough substrates, the perpendicular lamellae obtained after initial annealing changed to parallel lamellae after extended annealing [24,41]. The domain morphologies of cylinder-forming PS-*b*-PMMA films of $t \approx L_0$ ($=32 \sim 37$ nm) on Au/Si and Au/glass were thus investigated upon their annealing at higher temperature (190 °C) for a longer time (100 h, 150 h, 210 h).

Fig. 3 summarizes AFM images of PS-*b*-PMMA thin films on (a) Au/Si and (b) Au/glass that were annealed under different conditions. PMMA domains at the free surface of a PS-*b*-PMMA film on Au/Si were oriented horizontally after annealing at 190 °C for 150 h, in contrast to those oriented vertically after annealing at 170 °C for 60 h (Fig. 3(a)). The horizontal orientation of PMMA domains was similarly observed after annealing at 190 °C for 100 h. These observations indicated that the vertical orientation obtained upon annealing at 170 °C would be metastable. The PMMA domains were oriented horizontally to the underlying gold substrate at equilibrium due to the preferential affinity of PS fragments on gold surface [37,38].

On Au/glass, PS-*b*-PMMA films annealed at 190 °C for 150 h contained vertical domains at higher density than those at 170 °C for 60 h (Fig. 3(b)). However, PMMA domains were oriented horizontally in films annealed at 190 °C for 210 h (Fig. 3(b); right), indicating that the vertical orientation was obtained at the metastable state. The slower transition of the domain orientation on Au/glass would be due to its larger roughness amplitude as compared to Au/Si, which was consistent with the trend reported previously on the kinetics of roughness-induced domain orientation of lamella-forming PS-*b*-PMMA films [24].

3.4. Comparison of CVs on Au/Si and Au/glass coated with PS-*b*-PMMA-derived nanoporous films

A redox current measured using electrochemical methods reflects the diffusion of redox species onto the electrode in addition to the kinetics of the electron transfer reaction between the redox species and the electrode [42]. Thus, electrochemical methods have been used to characterize the geometry and surface properties of nanopores immobilized on electrode surfaces [32,43–47]. For example, using CV, we previously assessed the removal of the PMMA domains from thin (ca. 30 nm thick) PS-*b*-PMMA films on Au/Si, and identified the surface functional groups on PS-*b*-PMMA-derived nanopores [32]. We also employed CV to monitor changes in surface charge and effective pore diameter upon covalent functionalization of the nanopore surface [47] and to assess the penetration of redox-active biomolecules through the nanopores [48].

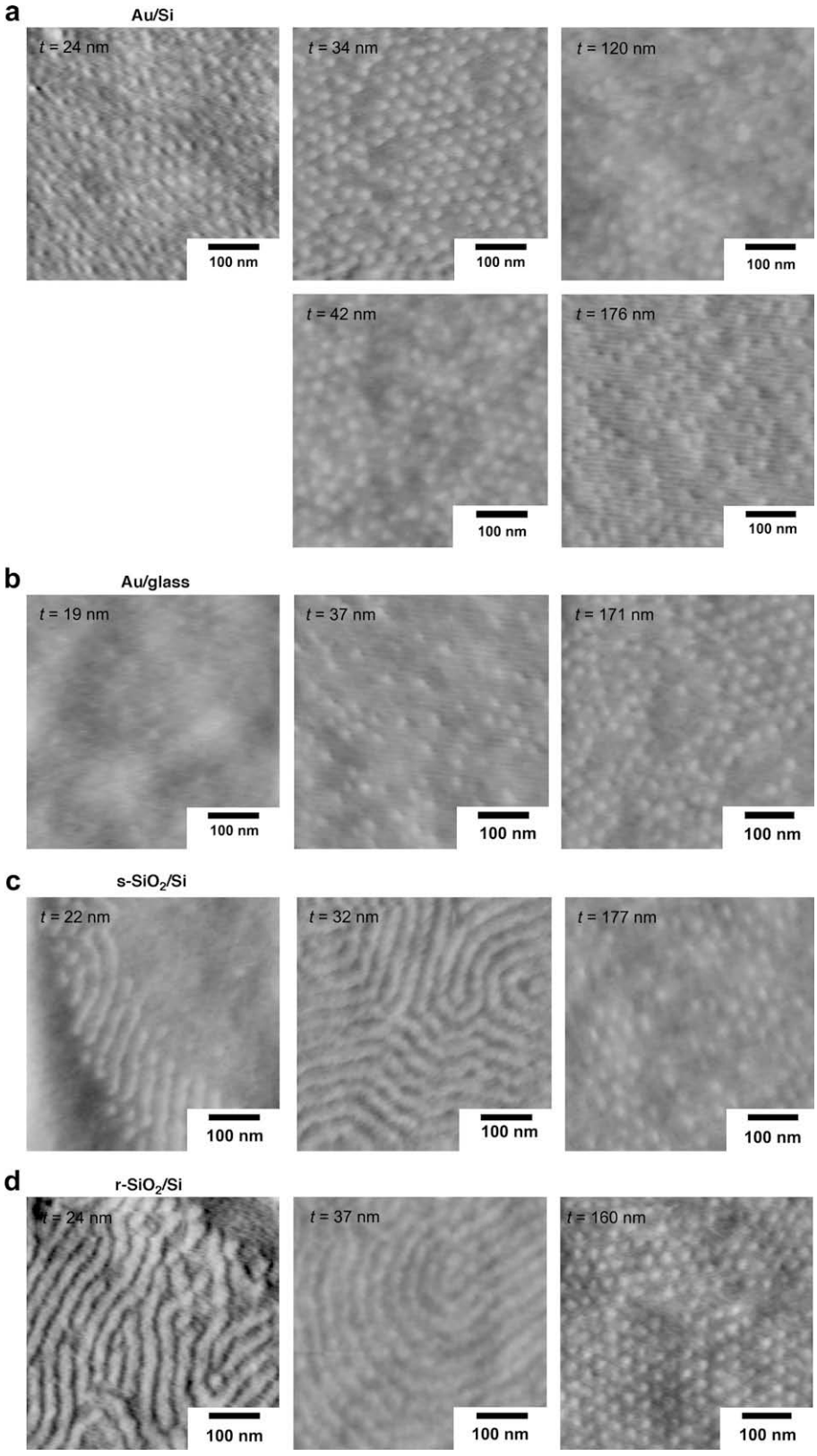

Fig. 2. AFM images ($500 \times 500\ nm^2$; $\Delta z = 20$ nm) of PS-*b*-PMMA film surfaces having different thicknesses (t) on (a) Au/Si, (b) Au/glass, (c) s-SiO_2/Si and (d) r-SiO_2/Si. The ellipsometric thickness of each film is included in each image. Left: $t < L_0$; center: $t \approx L_0$; right: $t \gg L_0$. All the PS-*b*-PMMA films were annealed at 160 °C for 60 h in vacuum.

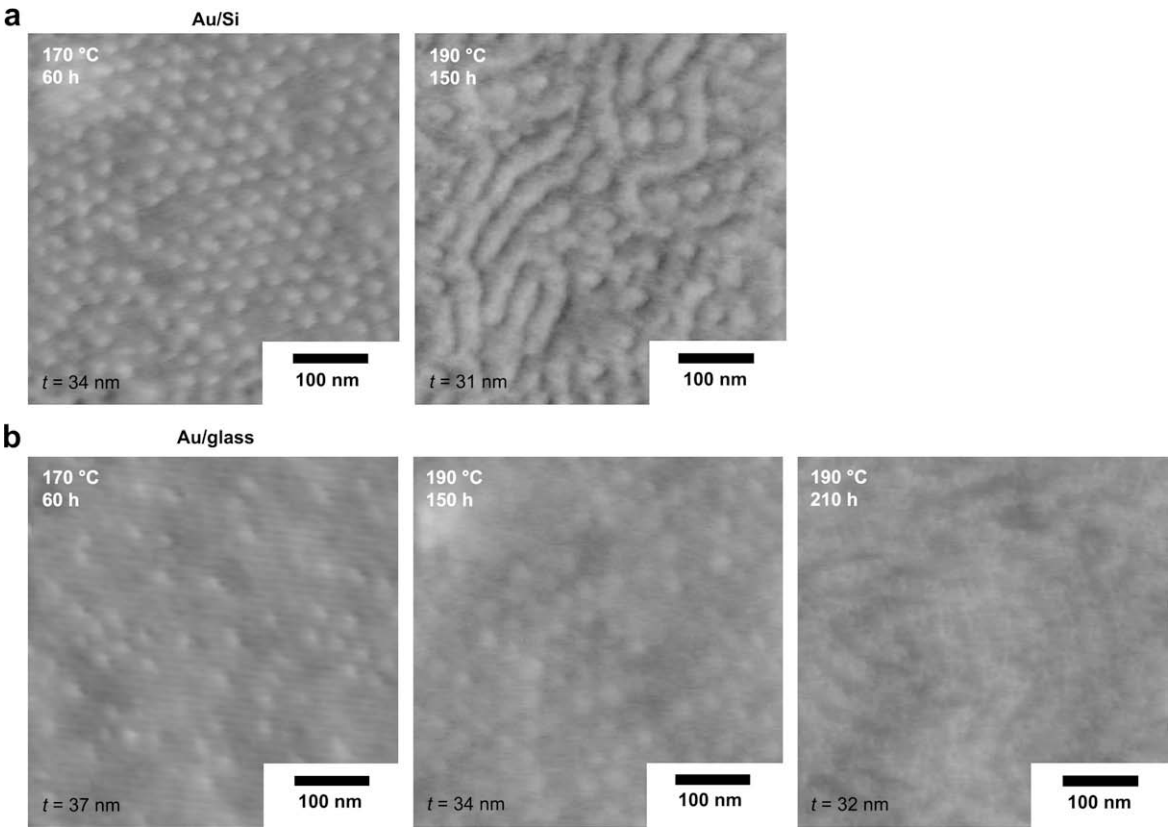

Fig. 3. AFM images (500×500 nm^2; $\Delta z = 20$ nm) of the surface of PS-*b*-PMMA films on (a) Au/Si and (b) Au/glass annealed under different conditions. The ellipsometric thickness of each film, which was close to L_0, is included in each image. The PS-*b*-PMMA films were annealed in vacuum at 160 °C for 60 h (left; the same images as those shown in Fig. 2(a) and (b)), at 190 °C for 150 h (center) and at 190 °C for 210 h (right).

Here, CVs of 1,1′-ferrocenedimethanol ($Fc(CH_2OH)_2$) were measured on Au/Si and Au/glass coated with PS-*b*-PMMA-derived nanoporous films having different thicknesses that were annealed at 170 °C for 60 h. The nanoporous films were obtained by etching out the PMMA domains from the PS-*b*-PMMA films via UV irradiation and subsequent sonication in AcOH. The domain orientation in the original (unetched) PS-*b*-PMMA films could be deduced from CV data that would reflect the nanoporous structure of the etched PS-*b*-PMMA films. Uncharged $Fc(CH_2OH)_2$ was used to assess the permeability of the nanoporous film with no influence of electrostatic interaction [32,47]. On the other hand, PS-*b*-PMMA films on SiO_2/Si could not be characterized using CV because of the insulating properties of the SiO_2 layer.

Fig. 4(a) shows CVs of $Fc(CH_2OH)_2$ on Au/Si and Au/glass coated with PS-*b*-PMMA-derived nanoporous films of $t \approx L_0$. The PMMA domains were etched to form cylindrical nanopores that would expose the underlying gold surface, allowing $Fc(CH_2OH)_2$ in the aqueous solution to diffuse to the electrode surface [32]. The peaks observed in these CVs, upon the potential sweep from 0 V to +0.5 V and from +0.5 V to 0 V (vs. Ag/AgCl), corresponded to the oxidation of $Fc(CH_2OH)_2$ that reached the underlying gold surface and the reduction of oxidized $Fc(CH_2OH)_2$ respectively. The maximum current on Au/Si substrates coated with the nanoporous films of $t \approx L_0$ was 50 ± 4 μA (scan rate: 0.05 V/s), which was similar to the peak current calculated using parameters obtained from the AFM images (the pore density: 900 pores/μm^2; pore radius: 10 nm), as reported previously [32]. This coincidence may suggest that most of the nanopores in the films, i.e., the PMMA domains in the original PS-*b*-PMMA films, on Au/Si reached the underlying gold surface [32]. Fig. 4(a) also shows that the Au/glass coated with the nanoporous film gave a slightly smaller redox current than the Au/Si coated with the nanoporous film. The smaller current on the Au/glass may be ascribed to the smaller density of vertically-aligned PMMA domains reaching the underlying gold substrate.

Fig. 4(b) shows CVs of $Fc(CH_2OH)_2$ for PS-*b*-PMMA-derived nanoporous films having different thicknesses on Au/Si. With increasing film thickness, the peak-shaped CVs changed to sigmoidal CVs. In addition, the maximum current decreased with increasing film thickness from 30 to 80 nm, and then reached a plateau (Fig. 4(c)). Similar trends were obtained for Au/glass substrates coated with nanoporous films having t between 30 nm and 100 nm (Fig. 4(c)). The observation of the peak-shaped CV at $t \approx L_0$ suggests that $Fc(CH_2OH)_2$ reached the underlying gold surface on the basis of linear diffusion resulting from the overlap of diffusion layers extending from individual nanopores at the time scale of the measurements (Fig. 4(d), left) [32,42]. In contrast, the observation of the sigmoidal CV at $t \gg L_0$ suggests that $Fc(CH_2OH)_2$ diffused radially from the outside of the nanopores (Fig. 4(d), right) [42,49]. Thus, the transition from peak-shaped to sigmoidal CVs with increasing film thickness probably reflected a decrease in the density of recessed nanoelectrodes exposed by the PMMA etching. The decrease in the nanoelectrode density increased the spacing between neighboring nanoelectrodes, and thus provided isolated radial diffusion layers from individual nanoelectrodes to give the sigmoidal CVs. Assuming the uniform distribution of the isolated recessed nanoelectrodes on the substrate, the density of open nanopores can be calculated from the limiting current in a sigmoidal CV (i_{lim}) using the following equation [49,50]:

$$i_{lim} = \frac{4\pi nFCDa^2N}{4L + \pi a} \quad (1)$$

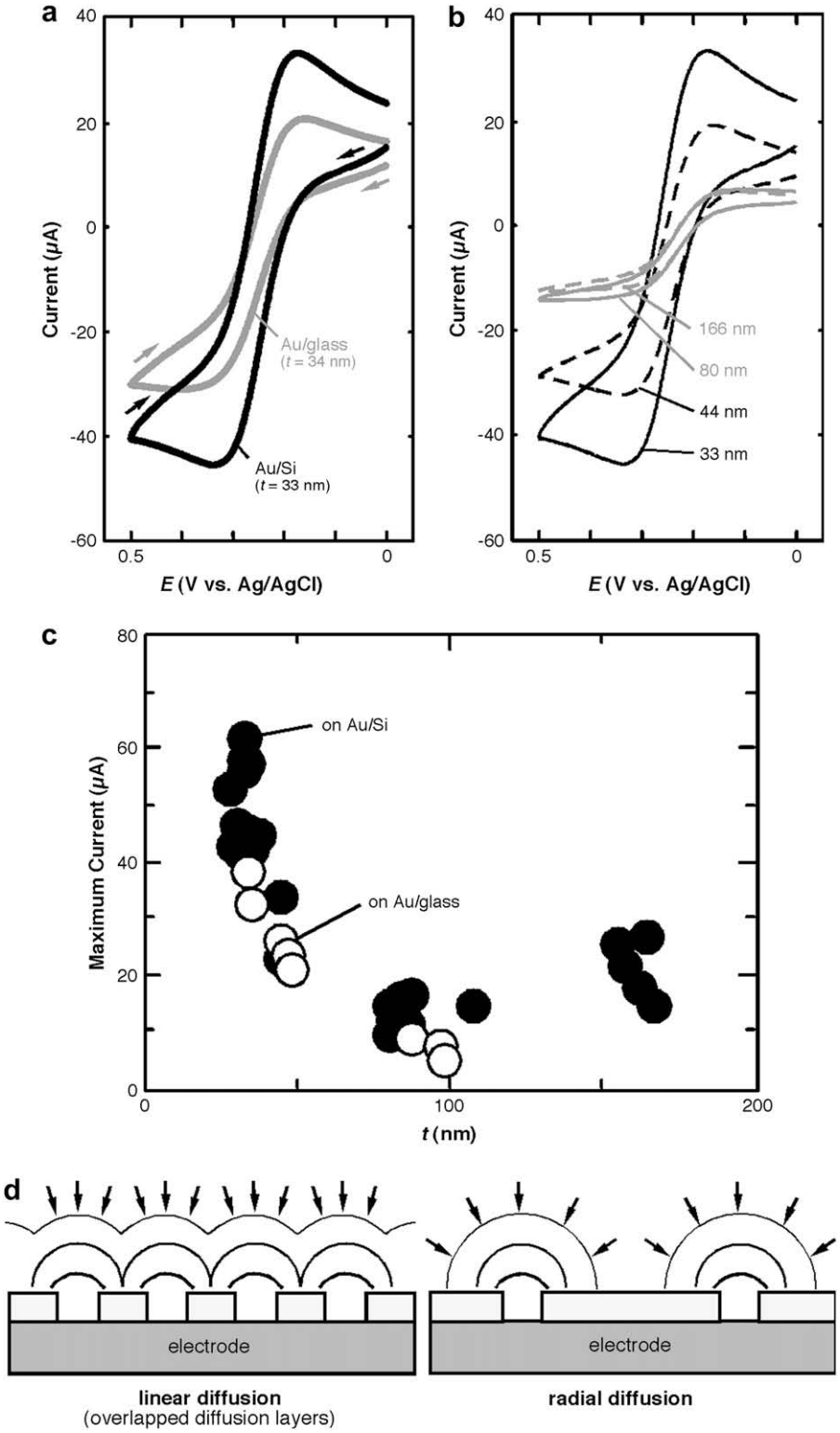

Fig. 4. (a) CVs (scan rate 0.05 V/s) of 3.0 mM $Fc(CH_2OH)_2$ in 0.1 M KNO_3 on Au/Si and Au/glass coated with PS-*b*-PMMA films ($t \approx L_0$) after the removal of the PMMA domains. (b) CVs (scan rate 0.05 V/s) of 3.0 mM $Fc(CH_2OH)_2$ in 0.1 M KNO_3 on Au/Si coated with PS-*b*-PMMA films having different t after the removal of the PMMA domains. (c) Maximum anodic current of $Fc(CH_2OH)_2$ in CVs (scan rate 0.05 V/s) on Au/Si (filled circles) and Au/glass (open circles) coated with PS-*b*-PMMA films having different t after the removal of the PMMA domains. All the PS-*b*-PMMA films were annealed at 170 °C for 60 h in vacuum. (d) Schematic illustrations of the linear diffusion mode due to the overlap of diffusion layers extending from individual nanopores (left) and the radial diffusion mode without the overlap (right).

In this equation, n is the number of electrons ($n = 1$ for $Fc(CH_2OH)_2$), F is Faraday's constant (=96,485 C/mol), R is the gas constant (=8.31 J/K · mol), T is temperature (=298 K for 25 °C), D is the diffusion coefficient of $Fc(CH_2OH)_2$ ($=6.4 \times 10^{-6}$ cm^2/s) [51], C (mol/cm^3) is its concentration ($=3.0 \times 10^{-6}$ mol/cm^3), a is pore radius ($\approx$10 nm), and L is the pore length ($\approx$film thickness). N, the number of the active nanoelectrodes, can be described as follows [49]:

$$N = \pi r^2 d \quad (2)$$

where r is the radius of the O-ring that defines the area in contact with the solution (=0.33 cm), and d is the density of the active nanoelectrodes.

For PS-*b*-PMMA-derived nanoporous films of $t \approx 170$ nm on Au/Si, the average limiting currents were 21 μA (Fig. 4(c)), giving $d = 6.0$ pores/μm^2. Although the effective inter-electrode spacing (=440 nm), calculated from d, was smaller than the thickness of the diffusion layer (≈26 μm at 0.05 V/s as scan rate) [42,49], the observation of the sigmoidal CVs would be possible since the inter-electrode spacing was >10 times larger than the pore diameter [52]. More importantly, this density value is much smaller than the density of vertical PMMA domains at the free surface (ca. 700 pores/μm^2; Fig. 2(a), right), suggesting that most of the PMMA domains exposed to the surface did not reach the underlying electrode. This is a sharp contrast to a nanoporous film of $t \approx L_0$ on Au/Si, which gave peak-shaped CVs whose peak currents were similar to that estimated from the pore density obtained from the corresponding AFM images (*vide supra*) [32]. This inconsistency observed on the PS-*b*-PMMA films of $t \gg L_0$ suggests that the domains would change their orientation and be interconnected inside the film. The interconnection of the microdomains may reflect the metastable nature of the domain orientation that is determined by the asymmetric boundary interactions at the polymer–vacuum interface in addition to those at the polymer–substrate interface [1]. Indeed, the interconnection of PMMA domains within lamella-forming PS-*b*-PMMA films in asymmetric systems was previously shown using cross-sectional transmission electron microscopy (TEM) [24,53].

4. Conclusions

This paper described the effects of substrate properties and film thickness on the orientation of cylindrical PMMA domains in thin films of PS-*b*-PMMA. The nanoscale roughness of gold substrates induced the metastable vertical orientation of PMMA domains at the polymer–substrate interface without neutralizing the block affinity of the substrate. The metastable vertical domain orientation was previously reported for lamella-forming, symmetric PS-*b*-PMMA films on indium tin oxide and polyimide substrates [23,24,27,28]. In contrast, regardless of their roughness, vertically oriented microdomains were not observed on oxide-coated Si substrates under the annealing conditions examined, probably because of the high affinity of PMMA fragments to the surface. However, more systematic investigations on the effects of substrate roughness, substrate block affinity and annealing conditions on the domain orientation would be necessary to fully understand the microdomain orientation in cylinder-forming PS-*b*-PMMA films on rough surfaces. According to the CV data, the vertical domains penetrated from the free surface to the substrate so that chemical etching of the PMMA domains resulted in the exposure of the underlying gold surface. However, in PS-*b*-PMMA films much thicker than its L_0, most of the vertical domains did not reach the underlying substrate maybe due to the metastable nature of the vertical domain orientation at the asymmetric boundary interactions. Thus, other approaches such as electric field application [6,12,22] would be required to obtain a high-density array of vertically oriented cylindrical domains in thicker films.

Acknowledgments

The authors thank Prof. Daniel A. Higgins (Department of Chemistry, Kansas State University) and Prof. Bruce Law (Department of Physics, Kansas State University) for the invaluable suggestions, and Ms. Shinobu Nagasaka for her assistance with PS-*b*-PMMA film preparation. The authors gratefully acknowledge the American Chemical Society Petroleum Research Fund, Kansas NSF EPSCoR grant, Terry C. Johnson Center for Basic Cancer Research and Kansas State University for financial support of this work.

References

[1] Fasolka MJ, Mayes AM. Annu Rev Mater Res 2001;31:323–55.
[2] Li M, Coenjarts CA, Ober CK. Adv Polym Sci 2005;190:183–226.
[3] Hillmyer MA. Adv Polym Sci 2005;190:137–81.
[4] Olson DA, Chen L, Hillmyer MA. Chem Mater 2008;20:869–90.
[5] Park M, Harrison C, Chaikin PM, Register RA, Adamson DH. Science 1997;276:1401–4.
[6] Thurn-Albrecht T, Schotter J, Kastle GA, Emley N, Shibauchi T, Krusin-Elbaum L, et al. Science 2000;290:2126–9.
[7] Kim H-C, Jia X, Stafford CM, Kim DH, McCarthy TJ, Tuominen M, et al. Adv Mater 2001;13:795–7.
[8] Darling SB, Yufa NA, Cisse AL, Bader SD, Sibener SJ. Adv Mater 2005;17:2446–50.
[9] Zhang Q, Xu T, Butterfield D, Misner MJ, Ryu DY, Emrick T, et al. Nano Lett 2005;5:357–61.
[10] Yang SY, Ryu I, Kim HY, Kim JK, Jang SK, Russell TP. Adv Mater 2006;18:709–12.
[11] Yang SY, Park J, Yoon J, Ree M, Jang SK, Kim JK. Adv Funct Mater 2008;18:1371–7.
[12] Thurn-Albrecht T, Steiner R, DeRouchey J, Stafford CM, Huang E, Bal M, et al. Adv Mater 2000;12:787–91.
[13] Mansky P, Russell TP, Hawker CJ, Pitsikalis M, Mays J. Macromolecules 1997;30:6810–3.
[14] Huang E, Russell TP, Harrison C, Chaikin PM, Register RA, Hawker CJ, et al. Macromolecules 1998;31:7641–50.
[15] Xu T, Kim H-C, DeRouchey J, Seney C, Levesque C, Martin P, et al. Polymer 2001;42:9091–5.
[16] Niemz A, Bandyopadhyay K, Tan E, Cha K, Baker SM. Langmuir 2006;22:11092–6.
[17] Mansky P, Liu Y, Huang E, Russell TP, Hawker C. Science 1997;275:1458–60.
[18] Fasolka MJ, Banerjee P, Mayes AM, Pickett G, Balazs AC. Macromolecules 2000;33:5702–12.
[19] Guarini KW, Black CT, Milkove KR, Sandstrom RL. J Vac Sci Technol B 2001;19:2784–8.
[20] Jeong U, Ryu DY, Kho DH, Kim JK, Goldbach JT, Kim DH, et al. Adv Mater 2004;16:533–6.
[21] Xuan Y, Peng J, Cui L, Wang H, Li B, Han Y. Macromolecules 2004;37:7301–7.
[22] Thurn-Albrecht T, DeRouchey J, Russell TP, Jaeger HM. Macromolecules 2000;33:3250–3.
[23] Sivaniah E, Hayashi Y, Iino M, Hashimoto T, Fukunaga K. Macromolecules 2003;36:5894–6.
[24] Sivaniah E, Hayashi Y, Matsubara S, Kiyono S, Hashimoto T, Fukunaga K, et al. Macromolecules 2005;38:1837–49.
[25] Sivaniah E, Matsubara S, Zhao Y, Hashimoto T, Fukunaga K, Kramer EJ, et al. Macromolecules 2008;41:2584–92.
[26] Podariu I, Chakrabarti A. J Chem Phys 2000;113:6423–8.
[27] Tsori Y, Andelman D. Macromolecules 2003;36:8560–6.
[28] Tsori Y, Sivaniah E, Andelman D, Hashimoto T. Macromolecules 2005;38:7193–6.
[29] Tomita N, Adachi S. J Electrochem Soc 2002;149:G245–50.
[30] Jeong U, Ryu DY, Kim JK, Kim DH, Russell TP, Hawker CJ. Adv Mater 2003;15:1247–50.
[31] Ito T, Forman SM, Cao C, Li F, Eddy Jr CR, Mastro MA, et al. Langmuir 2008;24:6630–5.
[32] Li Y, Maire HC, Ito T. Langmuir 2007;23:12771–6.
[33] Ron H, Matlis S, Rubinstein I. Langmuir 1998;14:1116–21.
[34] Williams R, Goodman AM. Appl Phys Lett 1974;25:531–2.
[35] Wu S. In: Brandrup J, Immergut EH, Grulke EA, Abe A, Bloch DR, editors. Polymer handbook. 4th ed. New York: John Wiley & Sons; 1999. p. 521–41.
[36] Gong Y, Joo W, Kim Y, Kim JK. Chem Mater 2008;20:1203–5.
[37] Feldman K, Tervoort T, PS, Spencer ND. Langmuir 1998;14:372–8.
[38] Lopes WA. Phys Rev E 2002;65:031606.
[39] Kim H-C, Russell TP. J Polym Sci B 2001;39:663–8.
[40] Ulman A. Chem Rev 1996;96:1533–54.
[41] Welander AM, Kang H, Stuen KO, Solak HH, Muller M, de Pablo JJ, et al. Macromolecules 2008;41:2759–61.
[42] Bard AJ, Faulkner LR. Electrochemical methods, fundamentals and applications. 2nd ed. New York: Wiley; 2001.
[43] Zhang B, Zhang Y, White HS. Anal Chem 2004;76:6229–38.
[44] Wang G, Zhang B, Wayment JR, Harris JM, White HS. J Am Chem Soc 2006;128:7679–86.
[45] Jeoung E, Galow TH, Schotter J, Bal M, Ursache A, Tuominen MT, et al. Langmuir 2001;17:6396–8.
[46] Laforgue A, Bazuin CG, Prud'homme RE. Macromolecules 2006;39:6473–82.
[47] Li Y, Ito T. Langmuir 2008;24:8959–63.
[48] Li Y, Ito T. Anal Chem 2009;81:851–5.
[49] Ito T, Audi AA, Dible GP. Anal Chem 2006;78:7048–53.
[50] Bond AM, Luscombe D, Oldham KB, Zoski CG. J Electroanal Chem 1988;249:1–14.
[51] Fan F-RF. J Phys Chem B 1998;102:9777–82.
[52] Bartlett PN, Taylor SL. J Electroanal Chem 1998;453:49–60.
[53] Sohn BH, Yun SH. Polymer 2002;43:2507–12.